Article

Theoretical Study of the Mechanism for the Reaction of Trimethylaluminum with Ozone

Megumi Kayanuma,* Yoong-Kee Choe, Takayuki Hagiwara, Naoto Kameda, and Yukihiro Shimoi

Cite This: *ACS Omega* 2021, 6, 26282−26292

Read Online

ACCESS | Metrics & More | Article Recommendations | SI Supporting Information

ABSTRACT: The mechanism for the reaction of trimethylaluminum (TMA, $Al(CH_3)_3$) with ozone (O_3) was investigated in detail using density functional theory calculations to understand the atomic layer deposition processes that form aluminum oxide surfaces. We examined the reactions of TMA and some possible intermediates with O_3 and revealed plausible paths to form methoxy ($-OCH_3$), formate ($-OCHO$), bicarbonate ($-CO_3H$), and hydroxyl ($-OH$) species. These species have been observed in previous experimental studies. It was shown that TMA easily reacts with O_3 to generate the $Al(CH_3)_2(OCH_3)(O_2)$ intermediate. The subsequent reaction between the OCH_3 and O_2 groups finally generated an intermediate having a formate group. When all of the CH_3 groups are converted into OCH_3 or $OCHO$, O_3 will react with these groups. In the latter reaction, bicarbonate was shown to be formed.
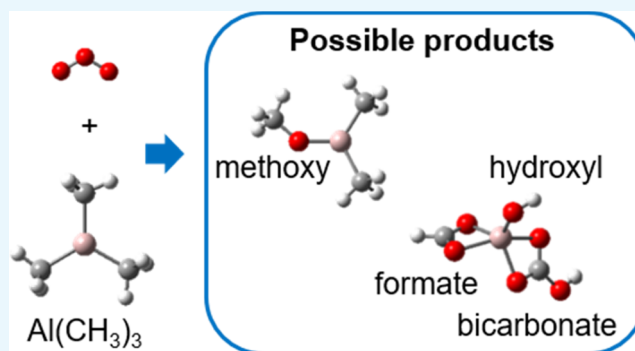
INTRODUCTION

Atomic layer deposition (ALD) is an important technique to develop high-quality nanomaterials with functional thin-film coatings, such as metals and metal oxides, for various applications such as electronics and catalysts.[1−3] ALD has several advantages compared with other deposition techniques: tunability of the film thickness and composition, good conformality and uniformity on the surface, high chemical selectivity, and industrial scalability. In the ALD process, the precursor is chemisorbed on surface functional groups (e.g., hydroxyl species) of the substrate material; then, the surface is exposed to the co-reactant, which reacts with the precursor chemisorbed on the surface, resulting in the formation of new surface functional groups. By repeating this cycle, the film grows.[1−3]

Trimethylaluminum (TMA, $Al(CH_3)_3$) is widely used as the precursor for ALD to form aluminum oxide (Al_2O_3) thin films. For the co-reactant, H_2O is often used.[4] However, ALD using H_2O molecules has several problems, for example, leaving unreacted hydroxyl groups in the generated Al_2O_3 films. Therefore, other co-reactants such as O_2 plasma and ozone (O_3) are also used.[3] It has been reported that ALD using O_3 reduced such defects[5,6] and the generated Al_2O_3 films had better insulating properties than those using H_2O as the co-reactant.[7]

To reveal the reaction mechanism involved in the ALD process using TMA precursor, many experimental studies have been reported.[8−12] For the gas-phase reaction of TMA with O_3, reaction intermediates have been analyzed at a low temperature (35 K) and room temperature, which showed the

formation of $Al(CH_3)_2(OCH_3)$, $Al(CH_3)_2(CHO)$, CH_3OO radical, CH_2O, CH_3OH, and C_2H_6.[8] For the ALD process using TMA and O_3, the formation of methoxy ($Al(OCH_3)$), formate ($Al(OCHO)$), bicarbonate ($Al(CO_3H)$), and hydroxyl ($Al(OH)$) species has been reported.[9] The authors proposed a reaction mechanism: two methoxy groups react and generate formate, which decomposes into CO and surface OH group at a high temperature or reacts with O_3 to form bicarbonate, and the bicarbonate decomposes to CO_2 and surface OH groups at high temperature. The reaction byproducts of the ALD process using TMA and O_3, CH_4, CO_2, and H_2O have been reported.[10] Rai et al. have shown that hydroxyl groups and carbonates (CO_3^{2-}) are generated during the ALD using TMA with O_2 plasma or O_3 and act as chemisorption sites for TMA.[11,12] Several theoretical analyses have also been conducted using density functional theory (DFT) calculations.[8,13−17] Al_2O_3 surfaces decorated with adsorbed methyl (CH_3) groups with singlet O atoms, which may come from the dissociation of O_3 or O_2 or from oxygen plasma, have been studied by Elliott et al.[13] Reactions of bare and hydroxylated alumina surfaces with TMA have also been reported.[14] Reactions of TMA with different types of surfaces,
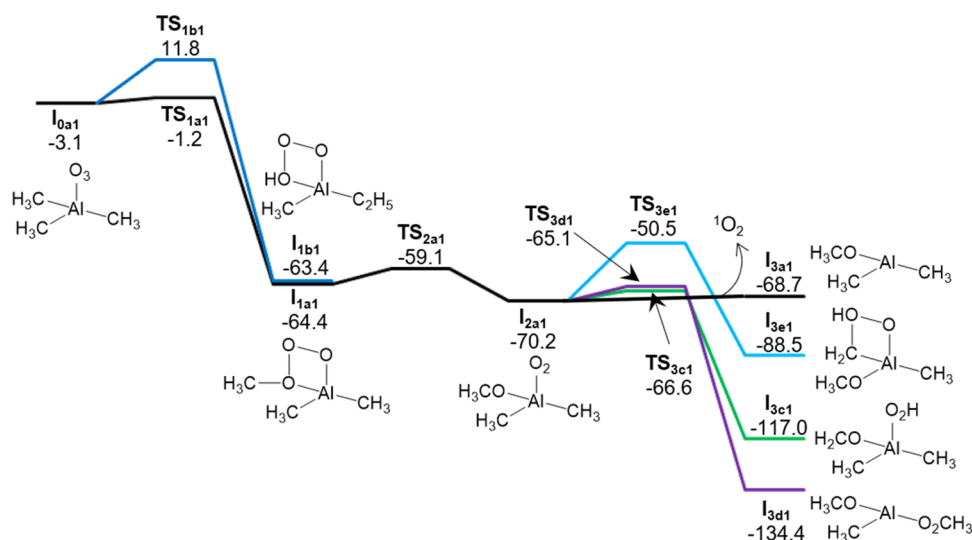
Figure 1. Free energy profiles of the initial steps of the reaction of $Al(CH_3)_3$ with O_3. The free energies are relative values to that of the separated pair of $Al(CH_3)_3$ and O_3 (in kcal/mol). For optimized structures, see Figure S1.

for example, $LiMn_2O_4$ surface[15] and carbon nanotubes,[16] have also been analyzed. About the gas-phase reactions, possible intermediates for the reaction of TMA with O_3 have been examined.[8] Nguyen et al. analyzed the mechanisms for the reactions of TMA with molecular oxygen and H_2O.[17]

Despite the previous works mentioned above, the details of the mechanism for the reaction of TMA with O_3 have not yet been revealed. In the present study, we revealed possible paths for the reaction of TMA with O_3 in the ALD process, which generates methoxy ($-OCH_3$), formate ($-OCHO$), bicarbonate ($-CO_3H$), and hydroxyl ($-OH$) species, using DFT calculations.

■ RESULTS AND DISCUSSION

$Al(CH_3)_3$ + O_3. The free energy profiles of the initial steps of the reaction between $Al(CH_3)_3$ and O_3 are shown in Figure 1. Their optimized structures, electronic energy, ro-vibrational parameters, and Cartesian coordinates are shown in Figure S1 and Tables S1, S2, and S3, respectively. When O_3 binds to $Al(CH_3)_3$, the free energy becomes lower than that of separated $Al(CH_3)_3$ and O_3 by 3.1 kcal/mol (I_{0a1}). For the first reaction step, two paths were examined, namely, the formation of a C−O bond (TS_{1a1}) or O−H bond (TS_{1b1}, a H atom of a CH_3 group is abstracted by the O_3 and the generated CH_2 group subsequently binds to a CH_3 group to form a CH_2CH_3 group). The former will be the dominant path because of the much lower activation barrier (1.9 kcal/mol) than that of the latter (14.9 kcal/mol), and the generated intermediate was lower in free energy than the reactant by −61.3 kcal/mol (I_{1a1} ($Al(CH_3)_2(O_3CH_3)$)). The O−O bond of the O_3CH_3 group in I_{1a1} dissociated easily because of the low activation energy (5.3 kcal/mol, TS_{2a1}), and an intermediate with a methoxy group was formed (I_{2a1} ($Al(CH_3)_2(OCH_3)(O_2)$), −70.2 kcal/mol). The methoxy group has been reported as an intermediate in the ALD process using TMA and O_3.[9] In this intermediate, O_2 coordinated to Al weakly, and when it was dissociated as a singlet O_2 molecule, the relative free energy increased only 1.5 kcal/mol (I_{3a1} ($Al(CH_3)_2(OCH_3)$) + $^1O_2$, −68.7 kcal/mol). Here, we do not consider intersystem crossing, which would generate a triplet O_2 molecule, because the present system

does not contain heavy elements and the spin−orbit coupling would be small. I_{3a1} has been reported as an intermediate in the gas-phase reaction of TMA with O_3 in a previous study.[8] Because I_{2a1} was much lower in free energy than the initial state ($Al(CH_3)_3$ + O_3) by −70.2 kcal/mol, such a dissociation reaction would be the main path in the gas-phase reaction due to the large internal energy, unless thermal relaxation is very efficient. The reaction of the I_{3a1} ($Al(CH_3)_2(OCH_3)$) intermediate to form $Al(CH_3)_2(CHO)$ + H_2, which was suggested in the previous experimental study of the gas-phase reaction,[8] is shown in Figure S2. When the O_2 was not released from I_{2a1}, it would be involved in the next reactions with OCH_3 or CH_3 groups. When O_2 moiety of I_{2a1} abstracted a H atom from the OCH_3 group (TS_{3c1}, activation energy was 3.6 kcal/mol), I_{3c1} ($Al(CH_3)_2(OCH_2)(O_2H)$, −117.0 kcal/mol) was generated. Another path, in which the second C−O bond was formed, had slightly higher activation energy (5.1 kcal/mol, TS_{3d1}) and generated I_{3d1} ($Al(CH_3)(OCH_3)(O_2CH_3)$, −134.4 kcal/mol). The reaction of the I_{3d1} ($Al(CH_3)(OCH_3)$-(O_2CH_3)) intermediate is shown in Figure S3. We also examined H abstraction from the CH_3 group by the O_2 moiety, but the activation energy was much higher (19.7 kcal/mol, TS_{3e1}) than for the other two transition states.

Figure 2 shows the free energy profiles of the reactions of the I_{3c1} ($Al(CH_3)_2(OCH_2)(O_2H)$) intermediate. The optimized structures are shown in Figure S4. The reaction between the OCH_2 and O_2H groups had low activation energy (9.3 kcal/mol, TS_{4c1}) and generated I_{4c1} ($Al(CH_3)_2(OCH_2O_2H)$). Then, the OH moiety of the OCH_2O_2H group coordinated to Al to form I_{5c1} (−122.0 kcal/mol), for which the reaction barrier was very low (1.6 kcal/mol, TS_{5c1}). From the I_{5c1} intermediate, we found two paths that had relatively low activation energies. At the lowest transition-state structure (TS_{6c1}, activation energy was 11.7 kcal/mol), dissociation of an O−O bond in the OCH_2O_2H group and migration of a H atom from a C atom to an O atom of the OCH_2O_2H group occurred simultaneously. The generated intermediate I_{6c1} ($Al(CH_3)_2(OCHOH)(OH)$, −195.2 kcal/mol), which contained formic acid, was much lower in energy than the previous intermediate (I_{5c1}, −122.0 kcal/mol). At another transition-state structure (TS_{6g1}), dissociation of an O−O bond of the
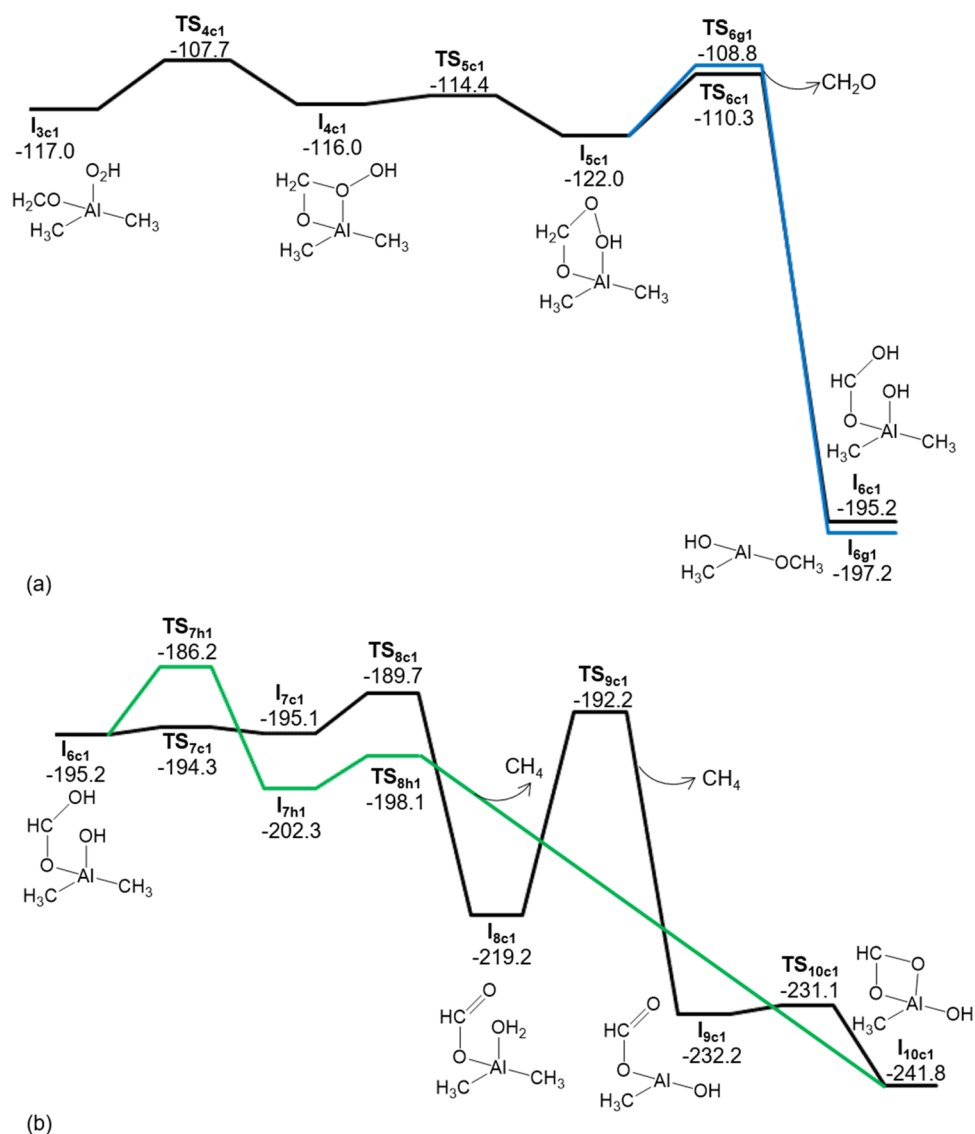
Figure 2. Free energy profiles of the reaction of (a) the I_{3c1} intermediate and (b) the I_{6c1} intermediate. The free energies are relative values to that of the separated pair of $Al(CH_3)_3$ and O_3 (in kcal/mol). For optimized structures, see Figure S4.
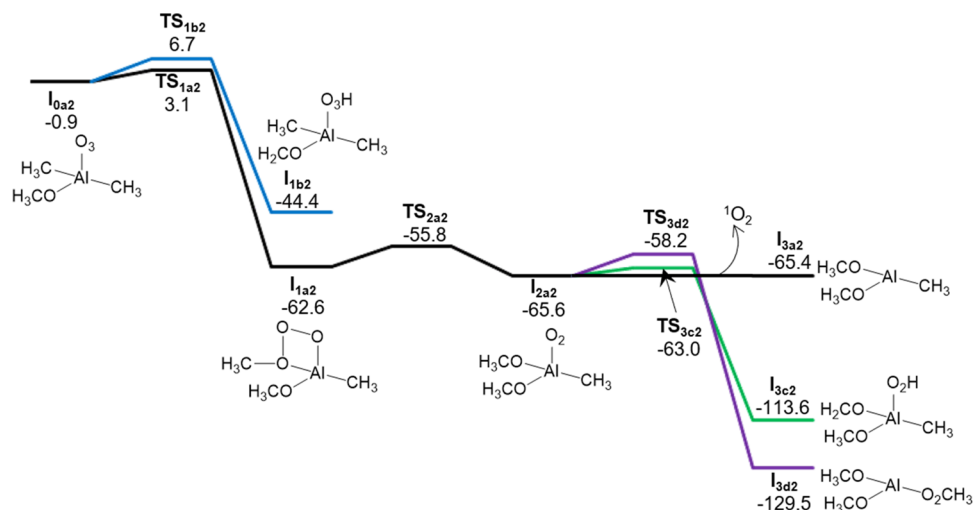

Figure 3. Free energy profiles of the initial steps of the reaction of $Al(CH_3)_2(OCH_3)$ with O_3. The free energies are relative values to that of the separated pair of $Al(CH_3)_2(OCH_3)$ and O_3 (in kcal/mol). For optimized structures, see Figure S5.

Figure 4. Free energy profiles of the reaction of $Al(CH_3)(OCHO)(OH)$ with O_3. The free energies are relative values to that of the separated pair of $Al(CH_3)(OCHO)(OH)$ and O_3 (in kcal/mol). For optimized structures, see Figure S7.
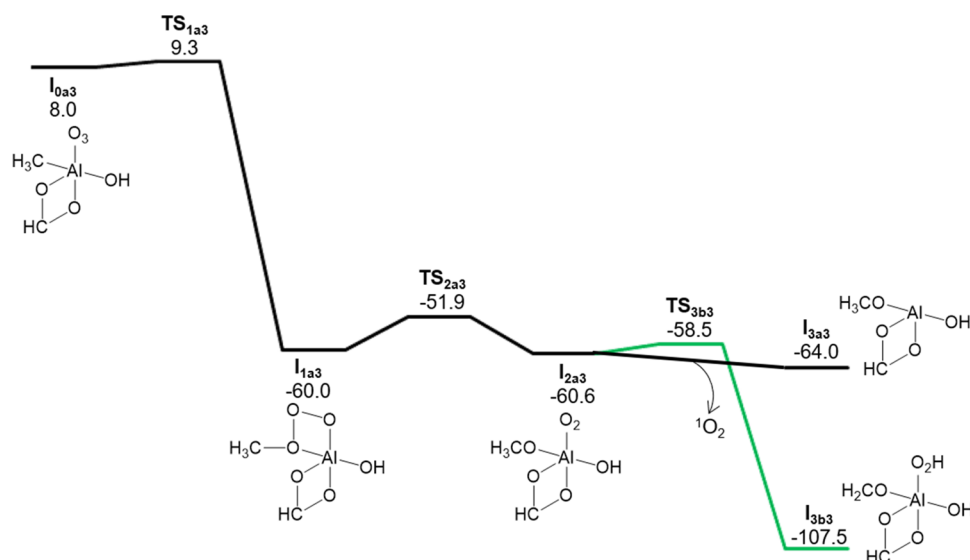
OCH_2O_2H group and C−O bond formation between a C atom of a CH_3 group and an O atom of an OCH_2O_2H group occurred simultaneously, which resulted in the formation of I_{6g1} $(Al(CH_3)(OCH_3)(OH))$ + CH_2O (−197.2 kcal/mol). The activation energy of this reaction (13.2 kcal/mol) was slightly higher than that of TS_{6c1}. After rotation of the OH group of I_{6c1} occurred (TS_{7c1}) to generate I_{7c1} (−195.1 kcal/mol), proton transfer from the OCHOH group to the OH group (TS_{8c1}, activation energy was 5.4 kcal/mol) occurred and generated I_{8c1} $(Al(CH_3)_2(OCHO)(OH_2))$, −219.2 kcal/mol). Then, proton transfer from the OH_2 group to the CH_3 group occurred (TS_{9c1}, activation energy of 27.0 kcal/mol), and I_{9c1} $(Al(CH_3)(OCHO)(OH))$ + CH_4 (−232.2 kcal/mol) was generated. When the monodentate OCHO group in I_{9c1} became the more stable bidentate form, I_{10c1} (−241.8 kcal/mol), the activation energy was very low (1.1 kcal/mol, TS_{10c1}). We also examined another path from the I_{6c1} $(Al(CH_3)_2(OCHOH)(OH))$ intermediate, which does not form an intermediate containing H_2O. In this path, rotation of the OH moiety in the OCHOH group occurred and generated I_{7h1} (−202.3 kcal/mol). The transition state for this reaction (TS_{7h1}, −186.2 kcal/mol) was higher than those in the other paths mentioned above (−194.3 and −189.7 kcal/mol at TS_{7c1} and TS_{8c1}, respectively). Then, proton transfer from the OCHOH group to the CH_3 group occurred (TS_{8h1}, activation energy was 4.2 kcal/mol), and generated I_{10c1} $(Al(CH_3)-(OCHO)(OH))$ + CH_4.

$Al(CH_3)_2(OCH_3)$ + O_3. We next examined the reaction of the I_{3a1} $(Al(CH_3)_2(OCH_3))$ intermediate with O_3. Figure 3 shows the free energy profiles of the initial steps of this reaction. The optimized structures are shown in Figure S5. When O_3 bound to $Al(CH_3)_2(OCH_3)$, the free energy became lower than that of separated $Al(CH_3)_2(OCH_3)$ and O_3 by 0.9 kcal/mol (I_{0a2}). Formation of a C−O bond had very low activation energy (4.0 kcal/mol, TS_{1a2}) and generated stable intermediate I_{1a2} $(Al(CH_3)(OCH_3)(O_3CH_3)$, −62.6 kcal/mol), as in the reaction of $Al(CH_3)_3$ with O_3. Another transition state, in which H abstraction from the OCH_3 group by O_3 occurred, had an activation energy of 7.6 kcal/mol ($TS1_{b2}$). Although $TS1_{b2}$ was higher in energy than $TS1_{a2}$, the

difference was only 3.6 kcal/mol; therefore, $TS1_{b2}$ would also contribute as a minor reaction path. In addition, when all of the CH_3 groups are reacted with O_3 and converted into a different functional group, such as an OCH_3 group, the reaction of the OCH_3 group with O_3 would occur. The reaction of I_{1a2} was similar to that of I_{1a1}. O−O bond dissociation occurred easily (TS_{2a2}, activation energy was 6.8 kcal/mol), which generated I_{2a2} $(Al(CH_3)(OCH_3)_2(O_2)$, −65.6 kcal/mol). From I_{2a2}, dissociation of a singlet O_2 molecule (formation of I_{3a2} $(Al(CH_3)(OCH_3)_2)$, −65.4 kcal/mol) or the reaction of O_2 with the OCH_3 or CH_3 groups would occur. H abstraction from the OCH_3 group by O_2, which formed I_{3c2} $(Al(CH_3)(OCH_3)(OCH_2)(O_2H)$, −113.6 kcal/mol), had a lower reaction barrier (2.4 kcal/mol, TS_{3c2}) than that of C−O bond formation between O_2 and CH_3 group (7.4 kcal/mol, TS_{3d2}), which formed I_{3d2} $(Al-(OCH_3)_2(O_2CH_3)$, −129.5 kcal/mol). The reaction of the I_{3c2} $(Al(CH_3)(OCH_3)(OCH_2)(O_2H))$ intermediate (Figure S6a) was also similar to that of I_{3c1} (Figure 2a).

Comparing the reactions of $Al(CH_3)_3$ and $Al-(CH_3)_2(OCH_3)$ with O_3, it was shown that their reactivities are similar. This indicates that the change of coordination environment does not significantly change the reactivity of other parts of the complex. Therefore, the results of the analyses of single molecules would be similar to that of TMA chemisorbed on the surface.

$Al(CH_3)(OCHO)(OH)$ + O_3. Figure 4 shows the free energy profile of the reaction of the I_{10c1} $(Al(CH_3)(OCHO)(OH))$ intermediate with O_3. The optimized structures are shown in Figure S7. When O_3 bound to $Al(CH_3)(OCHO)(OH)$, the free energy became higher than that of separated $Al(CH_3)-(OCHO)(OH)$ and O_3 by 8.0 kcal/mol (I_{0a3}) because of the very weak binding energy of O_3 to four-coordinated Al, which was smaller than the decrease of entropy. However, the following reaction was similar to that of $Al(CH_3)_3$ + O_3 and $Al(CH_3)_2(OCH_3)$ + O_3. After C−O bond formation, which had a very low activation energy (1.3 kcal/mol, TS_{1a3}) and generated the stable intermediate I_{1a3} $(Al(OCHO)(OH)-(O_3CH_3)$, −60.0 kcal/mol), O−O bond dissociation in the O_3CH_3 group occurred (TS_{2a3}, activation energy was 8.1 kcal/
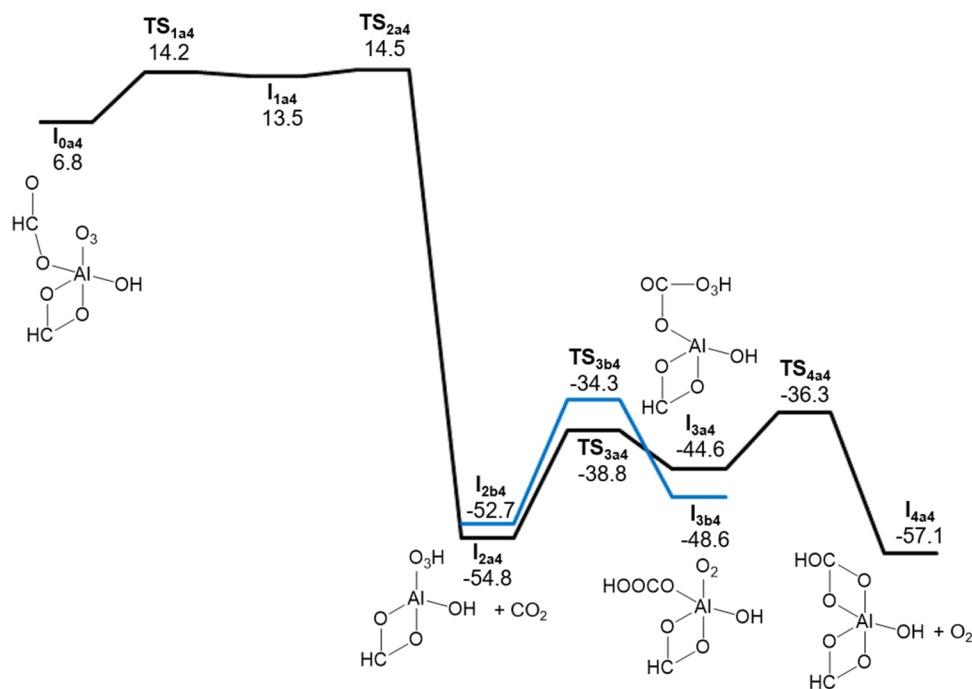
Figure 5. Free energy profiles of the reaction of $Al(OCHO)_2(OH)$ with O_3. The free energies are relative values to that of the separated pair of $Al(OCHO)_2(OH)$ and O_3 (in kcal/mol). For optimized structures, see Figure S9.
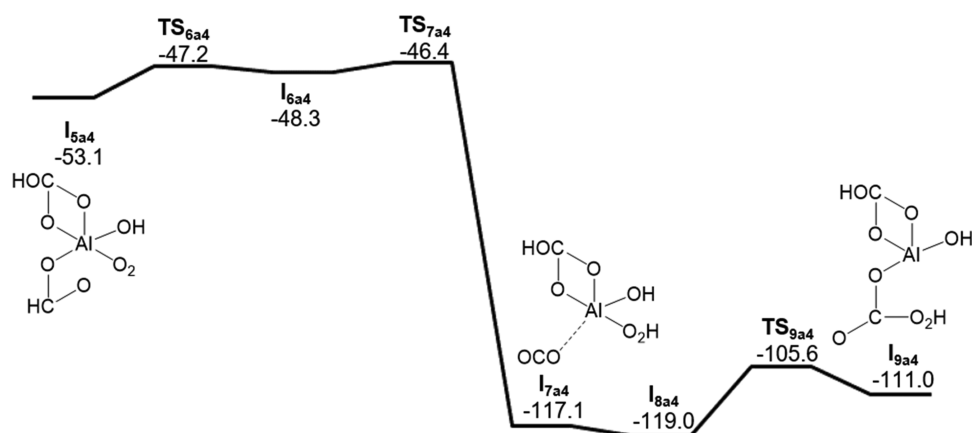

Figure 6. Free energy profiles of the reaction of the I_{5a4} intermediate, which differs from the I_{4a4} intermediate in the position of O_2 and the structure of $Al(OCHO)(OH)(CO_3H)$. The free energies are relative values to that of the separated pair of $Al(OCHO)_2(OH)$ and O_3 (in kcal/mol). For optimized structures, see Figure S10.

mol) and generated I_{2a3} ($Al(OCHO)(OH)(OCH_3)(O_2)$, −60.6 kcal/mol). Then, dissociation of a singlet O_2 molecule (formation of I_{3a3} ($Al(OCH_3)(OCHO)(OH)$) + $^1O_2$, −64.0 kcal/mol) or H abstraction from the OCH_3 group by O_2 (TS_{3b3}, activation energy was 2.1 kcal/mol) would occur, which generated I_{3b3} ($Al(OCHO)(OH)(OCH_2)(O_2H)$, −107.5 kcal/mol). The reaction of the I_{3b3} intermediate (Figure S8) was also similar to that of I_{3c1} (Figure 2) and I_{3c2} (Figure S6), except for the lack of a CH_3 group, which abstracted a proton from formic acid in the latter cases.

$Al(OCHO)_2(OH)$ + O_3. Figure 5 shows the free energy profiles of the reaction of I_{11b3} ($Al(OCHO)_2(OH)$), which was generated in the reaction of $Al(CH_3)(OCHO)(OH)$ + O_3 (Figure S8), with O_3. The optimized structures are shown in Figure S9. When O_3 bound to $Al(OCHO)_2(OH)$, the free energy became higher than that of separated $Al(OCHO)_2(OH)$ and O_3 by 6.8 kcal/mol (I_{0a4}) because of

the weak binding energy of O_3 to Al with high coordination number. In I_{0a4}, one of the OCHO groups became monodentate. Rotation of the monodentate OCHO group (TS_{1a4}, 14.2 kcal/mol) generated intermediate I_{1a4} (13.5 kcal/mol), in which abstraction of a H atom from the OCHO group by O_3 occurred easily (TS_{2a4}, 14.5 kcal/mol) and generated I_{2a4} ($Al(OCHO)(OH)(O_3H)$ + CO_2, −54.8 kcal/mol). Reaction between $Al(OCHO)(OH)(O_3H)$ and CO_2 generated I_{3a4} ($Al(OCHO)(OH)(OCO(O_3H))$, −44.6 kcal/mol), which required an activation energy of 16.0 kcal/mol (TS_{3a4}). Then, via the transition state with the $OCO(O_3H)$ group (TS_{4a4}, activation energy was 8.3 kcal/mol), proton transfer resulted in an intermediate having a bicarbonate group (I_{4a4} ($Al(OCHO)(OH)(CO_3H)$ + O_2), −57.1 kcal/mol). We also analyzed another possible path from the $Al(OCHO)(OH)$-(O_3H) + CO_2 intermediate, I_{2b4}, which differed in the position of CO_2 and conformation of $Al(OCHO)(OH)(O_3H)$ from
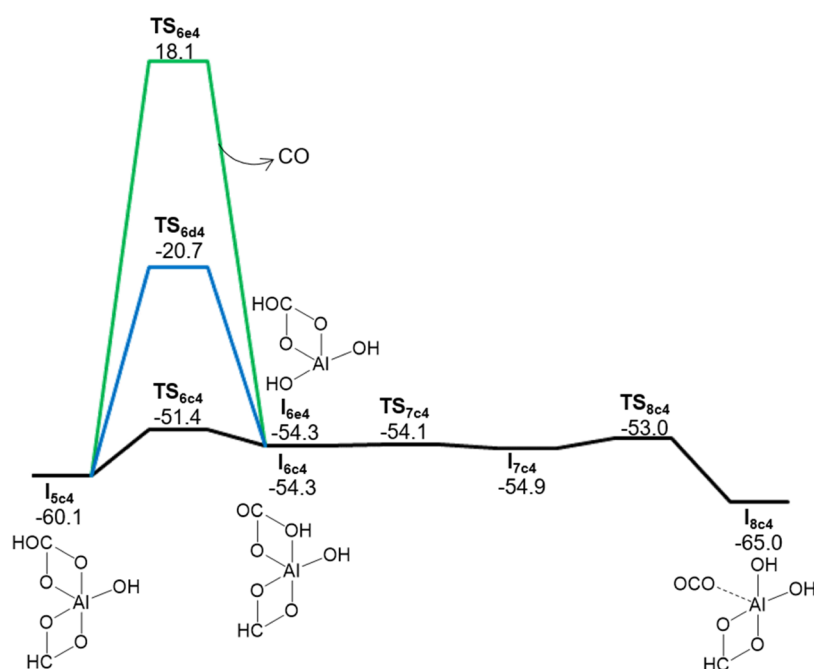
Figure 7. Free energy profiles of the reaction of the I_{5c4} intermediate, which was obtained by removal of a singlet O_2 molecule from the I_{4a4} intermediate. The free energies are relative values to that of the separated pair of $Al(OCHO)_2(OH)$ and O_3 (in kcal/mol). For optimized structures, see Figure S11.

Figure 8. Free energy profiles of the reaction of the I_{3f4} intermediate, which was obtained by removal of a CO_2 molecule from the I_{2a4} intermediate. The free energies are relative values to that of the separated pair of $Al(OCHO)_2(OH)$ and O_3 (in kcal/mol). For the optimized structure, see Figure S12.
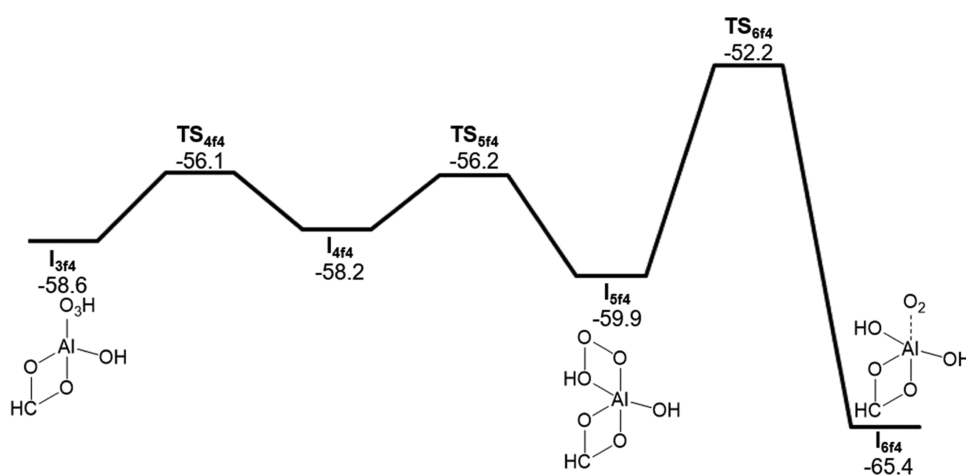
I_{2a4}. In this path, the OH moiety of the O_3H group reacted with CO_2 (TS_{3b4}, −34.3 kcal/mol) and generated I_{3b4} ($Al(OCHO)(OH)(CO_3H)(O_2)$, −48.6 kcal/mol). This transition state was slightly higher than that of TS_{3a4} (−38.8 kcal/mol).

Figure 6 shows the subsequent reaction of I_{4a4} when the generated O_2 reacted with $Al(OCHO)(OH)(CO_3H)$. The optimized structures are shown in Figure S10. When O_2 was coordinated to $Al(OCHO)(OH)(CO_3H)$ and the OCHO group became monodentate, the free energy increased (I_{5a4}, −53.1 kcal/mol). Rotation of the monodentate OCHO group (TS_{6a4}, −47.2 kcal/mol) generated intermediate I_{6a4} (−48.3 kcal/mol), from which abstraction of a H atom from the OCHO group by O_2 occurred easily (TS_{7a4}, −46.4 kcal/mol) and generated I_{7a4} ($Al(OH)(CO_3H)(O_2H) + CO_2$, −117.1 kcal/mol). These reactions are similar to that between the

OCHO group and O_3 shown in Figure 5 (from I_{0a4} to I_{2a4}). From I_{7a4} to I_{8a4}, the position of CO_2 changed and the conformation of $Al(OH)(CO_3H)(O_2H)$ changed. Reaction between $Al(OH)(CO_3H)(O_2H)$ and CO_2 (TS_{9a4}, activation energy was 13.4 kcal/mol) generated I_{9a4} ($Al(OH)(CO_3H)(OCO(O_2H))$, −111.0 kcal/mol). In the surface reaction, the $OCO(O_2H)$ group might react with some surface group or surface itself to generate carbonate.

From I_{4a4}, we also examined other paths, in which O_2 was released and decomposition of bicarbonate or formate occurred (Figure 7). The optimized structures are shown in Figure S11. Rotation of bicarbonate ligand occurred easily (TS_{6c4}, activation energy was 8.7 kcal/mol) because of weak binding of bicarbonate in five-coordinated structure. By contrast, proton transfer in the bicarbonate group required a high activation energy (39.4 kcal/mol, TS_{6d4}), so it would
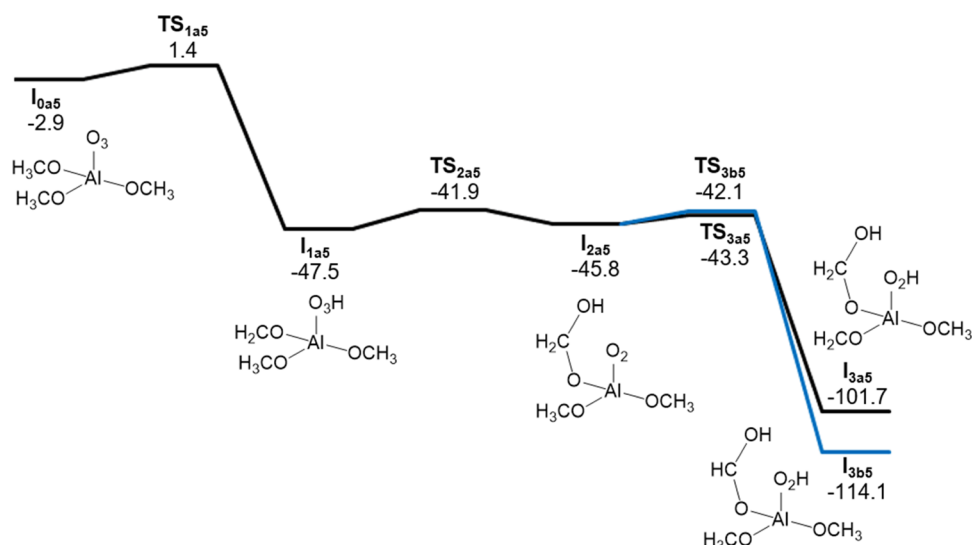
Figure 9. Free energy profiles of the initial steps of the reaction of $Al(OCH_3)_3$ with O_3. The free energies are relative values to that of the separated pair of $Al(OCH_3)_3$ and O_3 (in kcal/mol). For optimized structures, see Figure S13.
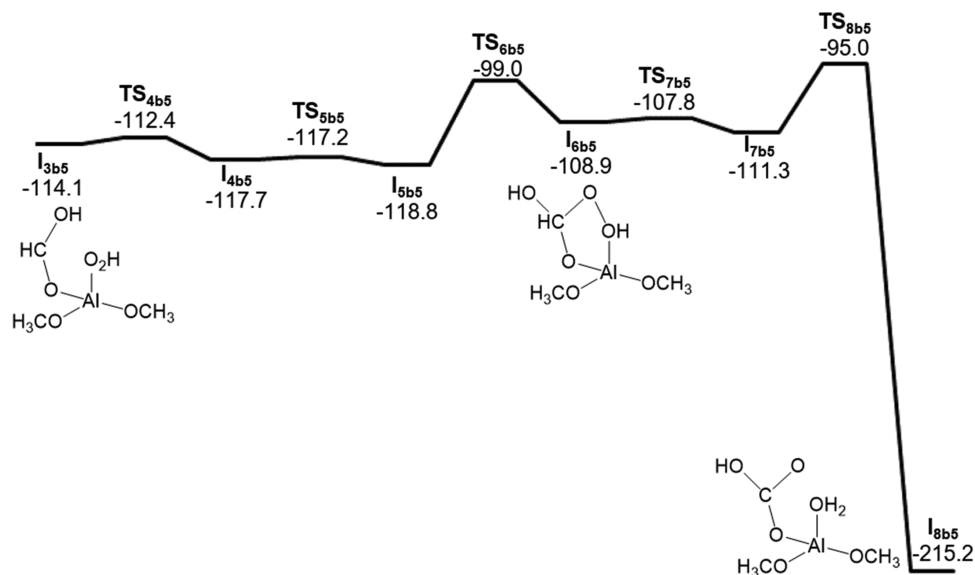

Figure 10. Free energy profiles of the initial steps of the reaction of the I_{3b5} intermediate. The free energies are relative values to that of the separated pair of $Al(OCH_3)_3$ and O_3 (in kcal/mol). For optimized structures, see Figure S14.

occur only at high temperatures. Through two low transition states (i.e., TS_{7c4} and TS_{8c4}, which correspond to the rotation of the OH group and dissociation of the C−O bond in the bicarbonate group, respectively), I_{8c4} ($Al(OCHO)(OH)_2$ + CO_2, −65.0 kcal/mol) was generated. We also examined the decomposition of formate to form CO and the OH group (I_{6e4} ($Al(OH)_2(CO_3H)$) + CO, −54.3 kcal/mol). However, the activation energy of this reaction was very high (78.2 kcal/mol, TS_{6e4}).

Figure 8 shows the reaction of the I_{3f4} intermediate, which occurred when CO_2 was released from the I_{2a4} intermediate in Figure 5. The optimized structures are shown in Figure S12. After rotation of O_3H (TS_{4f4}) and coordination of OH moiety in O_3H (TS_{5f4}), O_3H dissociated into O_2 and an OH group (TS_{6f4}, activation energy was 7.7 kcal/mol) and generated I_{6f4} ($Al(OH)_2(OCHO)$, −65.4 kcal/mol).

$Al(OCH_3)_3$ + O_3. In previous sections, we showed that O_3 reacted with the CH_3 group with low activation energy,

resulting in the formation of the OCH_3 group. Thus, we also examined the reaction of $Al(OCH_3)_3$ with O_3 (Figure 9) to reveal reactions that would occur when all of the CH_3 groups are already reacted with O_3. The optimized structures are shown in Figure S13. When O_3 bound to $Al(OCH_3)_3$, the free energy became lower than that of separated $Al(OCH_3)_3$ and O_3 by 2.9 kcal/mol (I_{0a5}). Abstraction of a H atom from the OCH_3 group by O_3 had a low activation barrier (4.3 kcal/mol, TS_{1a5}) and generated stable intermediate I_{1a5} ($Al(OCH_3)_2(OCH_2)(O_3H)$, −47.5 kcal/mol). The generated OCH_2 and O_3H groups reacted with low activation energy (5.6 kcal/mol, TS_{2a5}) and generated I_{2a5} ($Al(OCH_3)_2(OCH_2OH)$-(O_2), −45.8 kcal/mol). The generated O_2 group would abstract a H atom from the second OCH_3 group (TS_{3a5}, −43.3 kcal/mol) or OCH_2OH group (TS_{3b5}, −42.1 kcal/mol) and generate I_{3a5} ($Al(OCH_3)(OCH_2OH)(OCH_2)(O_2H)$, −101.7 kcal/mol) and I_{3b5} ($Al(OCH_3)_2(OCHO)(O_2H)$), respectively. Because I_{3a5} has OCH_2 and O_2H groups, like I_{3c1} (Figure 1),
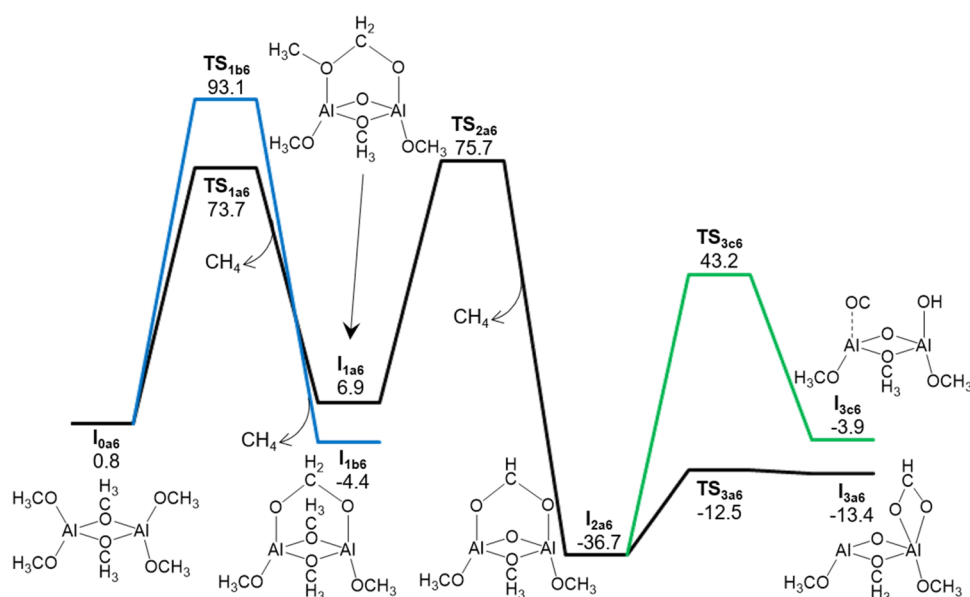
Figure 11. Free energy profiles of the reaction of $Al(OCH_3)_3$ dimer. The free energies are relative values to that of the most stable conformer of the dimer (in kcal/mol). For the optimized structure, see Figure S15.
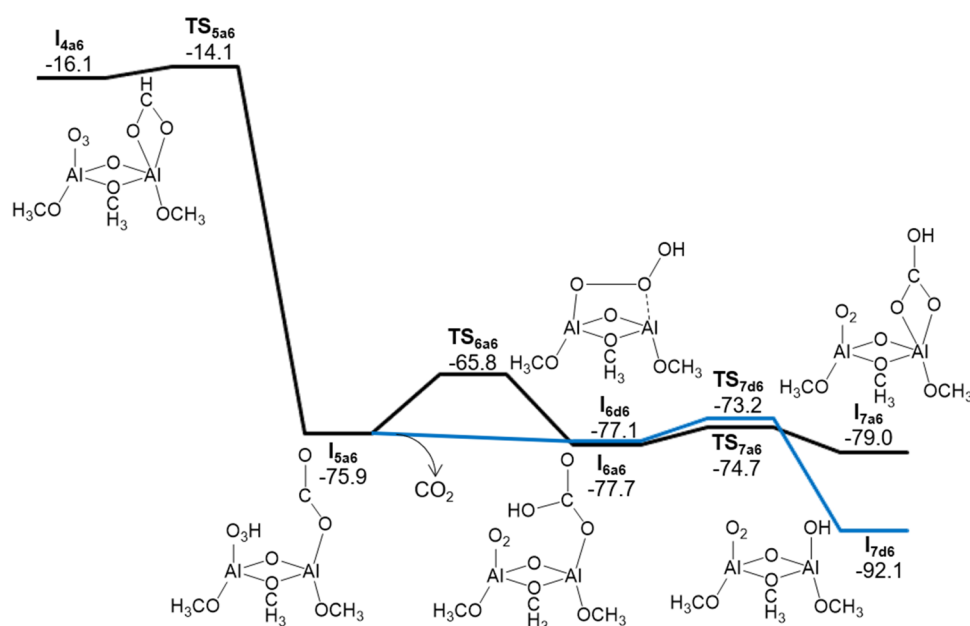

Figure 12. Free energy profiles of the reaction of the I_{3a6} intermediate with O_3. The free energies are relative values to that of the separated pair of the most stable conformer of the dimer and O_3 (in kcal/mol). For the optimized structures, see Figure S16.

I_{3c2} (Figure 3), and I_{3b3} (Figure 4), reactions similar to them (see Figures 2, S6, and S8) would occur and generate formate.

We examined the subsequent reaction of the I_{3b5} (Al-$(OCH_3)_2(OCHO)(O_2H)$) intermediate (Figure 10). The optimized structures are shown in Figure S14. After rotation of the OCHO group (TS_{4b5} and TS_{5b5}), which generated I_{5b5} (−118.8 kcal/mol), a reaction between the CHOH and O_2H groups occurred (TS_{6b5}, activation energy was 19.8 kcal/mol) and generated I_{6b5} (Al$(OCH_3)_2(OCHO(O_2H))$), −108.9 kcal/mol. After the conformational change of the OCHO(O_2H) group occurred (TS_{7b5}), dissociation of an O−O bond of the OCHO(O_2H) group and migration of a H atom from the C atom to an O atom in OCHO(O_2H) occurred simultaneously (TS_{8b5}, activation energy was 16.3 kcal/mol). An intrinsic

reaction coordinate (IRC) calculation showed that the H atom migrated to an O atom (which formed a transient structure, $Al(OCH_3)_2(CO_3H_2)(OH)$) and continued to migrate to another O atom, resulting in a stable intermediate containing bicarbonate, I_{8b5} (Al$(OCH_3)_2(CO_3H)(OH_2)$, −215.2 kcal/mol).

Al(OCH$_3$)$_3$ Dimer. In a previous study, the formation of formate from two surface OCH_3 groups (Al_s−OCH_3 + Al_s−OCH_3 → Al_s−$OCHO$−Al_s + CH_4 + 1/2H_2) was proposed.[9] To examine the reactivity of two ligands that bind to different Al atoms, we considered the reaction of $Al(OCH_3)_3$ dimer (Figures 11 and S15). In the dimer, two OCH_3 groups bridge the two Al atoms (bridging OCH_3 groups), and the other OCH_3 groups coordinate with one of the Al atoms (normal
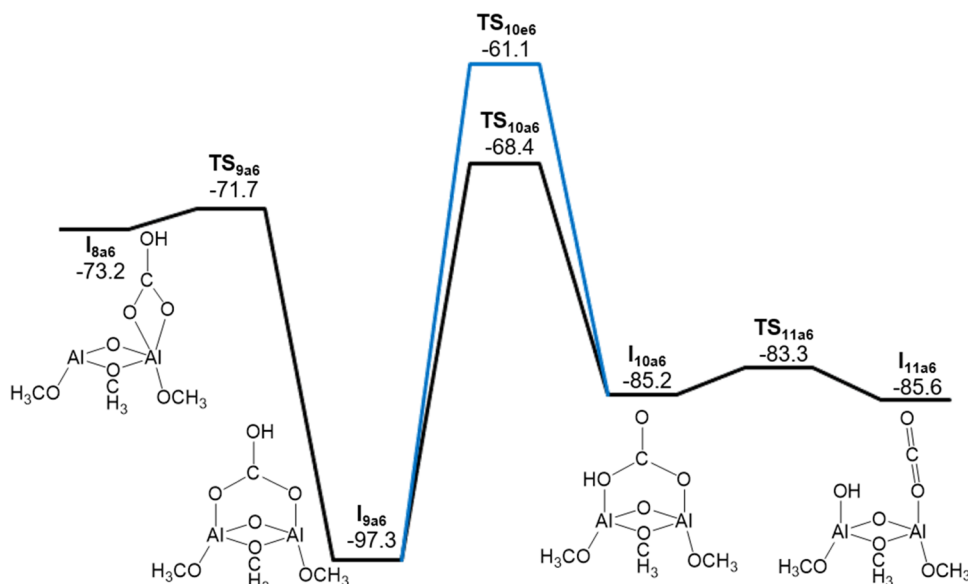
Figure 13. Free energy profiles of the reaction of the I_{8a6} intermediate, which was obtained after removal of a singlet O_2 molecule from the I_{7a6} intermediate. The free energies are relative values to that of the separated pair of the most stable conformer of the dimer (in kcal/mol). For the optimized structure, see Figure S17.

OCH$_3$ groups). We compared two paths in which a CH$_4$ molecule was generated from two OCH$_3$ groups, but both had high activation energies. The reaction between a normal OCH$_3$ group and a bridging OCH$_3$ group had a lower activation barrier (72.9 kcal/mol, TS$_{1a6}$) than that between two normal OCH$_3$ groups (92.3 kcal/mol, TS$_{1b6}$), although it was too high to overcome even at the high temperature used in ALD. The intermediate generated in the former path (I$_{1a6}$, 6.9 kcal/mol), in which the OCH$_2$ group bound to the OCH$_3$ group, was similar to the situation when one H atom ($1/2$H$_2$) is removed from a surface OCH$_3$ group; thus, we continued the analysis for this intermediate to examine whether CH$_4$ formation is plausible when a H atom is lost at the beginning. However, CH$_4$ formation from this intermediate also required high activation energy (68.8 kcal/mol, TS$_{2a6}$). Therefore, the reaction between two OCH$_3$ groups to form formate would not be plausible. To compare the decomposition of bridging formate with that of the chelate form (Figure 7), we analyzed the decomposition of I$_{2a6}$. The activation energy was 79.9 kcal/mol (TS$_{3c6}$), which was close to that of the chelate form (78.9 kcal/mol, TS$_{6d4}$) and generated CO and surface OH (I$_{3c6}$, −3.9 kcal/mol), which was much higher in energy than that of formate (I$_{2a6}$, −36.7 kcal/mol). We also analyzed a reaction in which formate moved to a single Al atom (TS$_{3a6}$) and generated an open Al site (I$_{3a6}$, −13.4 kcal/mol), where other molecules can bind, to examine the reaction between formate and O$_3$ bound to different Al sites.

Figure 12 shows the reaction of surface formate and O$_3$, which are coordinated to different Al atoms. The optimized structures are shown in Figure S16. The reactivity was similar to the reaction between formate and O$_3$ bound to the same Al atom (Figure 5). O$_3$ can abstract a H atom from the formate group easily (TS$_{5a6}$, activation energy was 2.0 kcal/mol) and generate an intermediate having CO$_2$ and O$_3$H groups (I$_{5a6}$, −75.9 kcal/mol), similar to the reaction of the monomer (Figure 5), although CO$_2$ and O$_3$H bind to a different Al atom in this case. Then, a reaction between CO$_2$ and O$_3$H occurred (TS$_{6a6}$, activation energy was 10.1 kcal/mol) and generated

bicarbonate and O$_2$ (I$_{6a6}$, −77.7 kcal/mol). The generated monodentate bicarbonate would become the bidentate form (I$_{7a6}$) via a low transition state (TS$_{7a6}$, activation energy was 3.0 kcal/mol). When CO$_2$ was released from I$_{5a6}$, the O$_3$H group dissociated into O$_2$ + OH via a low transition state (TS$_{7d6}$, activation energy was 3.9 kcal/mol).

We also examined the decomposition of bicarbonate in a bridging ligand form. Figure 13 shows the decomposition of bicarbonate in I$_{7a6}$ after O$_2$ was dissociated (I$_{8a6}$). The optimized structures are shown in Figure S17. The bicarbonate became a bridging ligand easily (TS$_{9a6}$, activation energy was 1.5 kcal/mol). It was shown that the activation energy of the proton transfer in the bridging bicarbonate (36.2 kcal/mol, TS$_{10e6}$) was similar to that of chelate bicarbonate (39.4 kcal/mol, TS$_{6d4}$ shown in Figure 7); by contrast, the rotation of bicarbonate ligand had much higher activation energy (28.9 kcal/mol, TS$_{10a6}$) than that of chelate bicarbonate (8.7 kcal/mol, TS$_{6c4}$). Thus, the bridging bicarbonate would be stable and would decompose only at high temperatures.

■ CONCLUSIONS

We analyzed the mechanism for the reaction of TMA with O$_3$ using DFT calculations. It was shown that Al(CH$_3$)$_3$ easily reacted with O$_3$ to generate Al(CH$_3$)$_2$(OCH$_3$)(O$_2$), I$_{2a1}$. When the generated O$_2$ was not released from this intermediate and involved in subsequent reactions, the O$_2$ group reacted with the OCH$_3$ group to form the Al(CH$_3$)$_2$(OCH$_2$)(O$_2$H) intermediate (I$_{3c1}$) and finally generated formate species, Al(CH$_3$)(OCHO)(OH) + CH$_4$ (I$_{9c1}$ or I$_{10c1}$). When O$_3$ reacted with an intermediate having both CH$_3$ and OCH$_3$ groups, i.e., Al(CH$_3$)$_2$(OCH$_3$) (I$_{3a1}$), O$_3$ would react with the CH$_3$ group preferentially (TS$_{1a2}$), although the reaction with OCH$_3$ also had a low activation barrier (TS$_{1b2}$), which was higher than that of the former by 3.6 kcal/mol. When all of the CH$_3$ groups are converted into OCH$_3$ or OCHO, O$_3$ will react with these groups. In the former case, the reaction between the OCH$_3$ group and O$_3$ generated an intermediate having the OCH$_2$OH group (Al(OCH$_3$)$_2$(OCH$_2$OH)(O$_2$), I$_{2a5}$), which

would finally generate formate or bicarbonate species. When O_3 reacted with formate, bicarbonate was obtained. The formation of formate from reactions between two OCH_3 groups, which was proposed in a previous study,[9] was shown to be unlikely (Figure 11).

Comparing the reactions of $Al(CH_3)_3$ + O_3 (Figure 1), $Al(CH_3)_2(OCH_3)$ + O_3 (Figure 3), and $Al(CH_3)(OCHO)$-(OH) + O_3 (Figure 4), the coordination environment does not significantly affect the reactivity of each ligand. Therefore, similar reactions are expected to occur also at the surface, and the reaction mechanisms for the monomers revealed comprehensibly in the present study will provide insights to understand the chemical processes in ALD.

■ THEORETICAL METHODS

The mechanism for the reaction of $Al(CH_3)_3$ with O_3 was analyzed using DFT calculations with the B3LYP functional[18,19] and 6-311G(d,p) basis sets.[20,21] The effects of basis set and functionals were also examined for some intermediates and transition states (Table S1). We also considered the reactions of some intermediates that would be generated from the $Al(CH_3)_3$ + O_3 reaction, such as $Al(CH_3)_2(OCH_3)$. To examine the reactions between two ligands coordinated to different Al atoms, reactions of the $Al(OCH_3)_3$ dimer model were also analyzed. In total, we analyzed the reactions of six reactants with O_3, and several paths were examined for each reactant. Notations of the intermediate and transition-state structures in each path are I_{xyz} and TS_{xyz}, respectively, where x, y, and z indicate the number of each reaction step (1, 2, 3, ...), the notation of the path (a, b, c, ...), and the notation for the reactant (1−6). Frequency calculations were performed for all calculated structures to confirm they are true minima or transition states, and the potential energy profiles shown below are of Gibbs free energy at 298.15 K. Intrinsic reaction coordinate (IRC) calculations were carried out for the transition states to confirm the minima structures. The calculations were performed using Gaussian 16 quantum chemistry software.[22]

■ ASSOCIATED CONTENT

Ⓢ Supporting Information

The Supporting Information is available free of charge at https://pubs.acs.org/doi/10.1021/acsomega.1c03326.

Optimized structures and the Cartesian coordinates; electronic energies calculated using different methods and ro-vibrational parameters of the intermediates and transition states shown in Figure 1; and free energy profiles of the reactions of the I_{3a1}, I_{3d1}, I_{3c2}, and I_{3b3} intermediates (PDF)

■ AUTHOR INFORMATION

Corresponding Author

Megumi Kayanuma − *Research Center for Computational Design of Advanced Functional Materials, National Institute of Advanced Industrial Science and Technology, Tsukuba, Ibaraki 305-8568, Japan;* ⓘ orcid.org/0000-0003-1149-5857; Email: m.kayanuma@aist.go.jp

Authors

Yoong-Kee Choe − *Research Center for Computational Design of Advanced Functional Materials, National Institute*

of Advanced Industrial Science and Technology, Tsukuba, Ibaraki 305-8568, Japan

Takayuki Hagiwara − *Meiden Nanoprocess Innovations, Inc., Chiba, Chiba 262-0013, Japan*

Naoto Kameda − *Meiden Nanoprocess Innovations, Inc., Chiba, Chiba 262-0013, Japan*

Yukihiro Shimoi − *Research Center for Computational Design of Advanced Functional Materials, National Institute of Advanced Industrial Science and Technology, Tsukuba, Ibaraki 305-8568, Japan;* ⓘ orcid.org/0000-0001-8108-2244

Complete contact information is available at:
https://pubs.acs.org/10.1021/acsomega.1c03326

Notes

The authors declare no competing financial interest.

■ ACKNOWLEDGMENTS

■ REFERENCES

(1) Mallick, B. C.; Hsieh, C.-T.; Yin, K.-M.; Gandomi, Y. A.; Huang, K.-T. Review−on atomic layer deposition: current progress and future challenges. *ECS J. Solid State Sci. Technol.* **2019**, *8*, N55−N78.

(2) Meng, X.; Wang, X.; Geng, D.; Ozgit-Akgun, C.; Schneider, N.; Elam, J. W. Atomic layer deposition for nanomaterial synthesis and functionalization in energy technology. *Mater. Horiz.* **2017**, *4*, 133−154.

(3) Potts, S. E.; Kessels, W. M. M. Energy-enhanced atomic layer deposition for more process and precursor versatility. *Coord. Chem. Rev.* **2013**, *257*, 3254−3270.

(4) Puurunen, R. L. Surface chemistry of atomic layer deposition: a case study for the trimethylaluminum/water process. *J. Appl. Phys.* **2005**, *97*, No. 121301.

(5) Kim, J. B.; Kwon, D. R.; Chakrabarti, K.; Leee, C.; Oh, K. Y.; Lee, J. H. Improvement in Al_2O_3 dielectric behavior by using ozone as an oxidant for the atomic layer deposition technique. *J. Appl. Phys.* **2002**, *92*, 6739−6742.

(6) Kim, S. K.; Lee, S. W.; Hwang, C. S.; Min, Y.-S.; Won, J. Y.; Jeong, J. Low temperature (<100°C) deposition of aluminum oxide thin films by ALD with O_3 as oxidant. *J. Electrochem. Soc.* **2006**, *153*, F69−F76.

(7) Nikolaou, N.; Ioannou-Sougleridis, V.; Dimitrakis, P.; Normand, P.; Skarlatos, D.; Giannakopoulos, K.; Kukli, K.; Niinistö, J.; Ritala, M.; Leskelä, M. The effect of oxygen source on atomic layer deposited Al_2O_3 as blocking Oxide in metal/auminum oxide/nitride/oxide/silicon memory capacitors. *Thin Solid Films* **2013**, *533*, 5−8.

(8) Sriyarathne, H. D. M.; Ault, B. S. Matrix isolation studies of novel intermediates in the reaction of trimethylaluminum with ozone. *J. Phys. Chem. A* **2017**, *121*, 7335−7342.

(9) Goldstein, D. N.; McCormick, J. A.; George, S. M. Al_2O_3 atomic layer deposition with trimethylaluminum and ozone studied by in situ transmission FTIR spectroscopy and quadrupole mass spectrometry. *J. Phys. Chem. C* **2008**, *112*, 19530−19539.

(10) Rose, M.; Niinistö, J.; Endler, I.; Bartha, J. W.; Kücher, P.; Ritala, M. In situ reaction mechanism studies on ozone-based atomic layer deposition of Al_2O_3 and HfO_2. *ACS Appl. Mater. Interfaces* **2010**, *2*, 347−350.

(11) Rai, V. R.; Vandalon, V.; Agarwal, S. Surface reaction mechanisms during ozone and oxygen plasma assisted atomic layer deposition of aluminum oxide. *Langmuir* **2010**, *26*, 13732−13735.

(12) Rai, V. R.; Vandalon, V.; Agarwal, S. Influence of surface temperature on the mechanism of atomic layer deposition of

aluminum oxide using oxygen plasma and ozone. *Langmuir* **2012**, *28*, 350−357.

(13) Elliott, S. D.; Scarel, G.; Wiemer, C.; Fanciulli, M.; Oavia, G. Ozon-based atomic layer deposition of alumina from TMA: growth, morphology, and reaction mechanism. *Chem. Mater.* **2006**, *18*, 3764−3773.

(14) Elliott, S. D.; Greer, J. C. Simulating the atomic layer deposition of alumina from first principles. *J. Mater. Chem.* **2004**, *14*, 3246−3250.

(15) Chen, L.; Warburton, R. E.; Chen, K.-S.; Libera, J. A.; Johnson, C.; Yang, Z.; Hersam, M. C.; Greeley, J. P.; Elam, J. W. Mechanism for Al_2O_3 atomic layer deposition on $LiMn_2O_4$ from in situ measurements and ab initio calculations. *Chem* **2018**, *4*, 2418−2435.

(16) Förster, A.; Wagner, C.; Schuster, J.; Friedrich, J. Ab initio study of the trimethylaluminum atomic layer deposition process on carbon nanotubes−an alternative initial step. *J. Vac. Sci. Technol. A* **2017**, *35*, No. 01B133.

(17) Nguyen, H. M. T.; Tang, H.-Y.; Huang, W.-F.; Lin, M. C. Mechanisms for reactions of trimethylaluminum with molecular oxygen and water. *Comput. Theor. Chem.* **2014**, *1035*, 39−43.

(18) Becke, A. D. Density-functional thermochemistry. III. The role of exact exchange. *J. Chem. Phys.* **1993**, *98*, 5648−5652.

(19) Lee, C.; Yang, W.; Parr, R. G. Development of the Colle-Salvetti correlation-energy formula into a functional of the electron density. *Phys. Rev. B* **1988**, *37*, 785−789.

(20) Krishnan, R.; Binkley, J. S.; Seeger, R.; Pople, J. A. Self-consistent molecular orbital methods. XX. A basis set for correlated wave functions. *J. Chem. Phys.* **1980**, *72*, 650−654.

(21) McLean, A. D.; Chandler, G. S. Contracted Gaussian basis sets for molecular calculations. I. Second row atoms, Z=11-18. *J. Chem. Phys.* **1980**, *72*, 5639−5648.

(22) Frisch, M. J.; Trucks, G. W.; Schlegel, H. B.; Scuseria, G. E.; Robb, M. A.; Cheeseman, J. R.; Scalmani, G.; Barone, V.; Petersson, G. A.; Nakatsuji, H.; Li, X.; Caricato, M.; Marenich, A. V.; Bloino, J.; Janesko, B. G.; Gomperts, R.; Mennucci, B.; Hratchian, H. P.; Ortiz, J. V.; Izmaylov, A. F.; Sonnenberg, J. L.; Williams-Young, D.; Ding, F.; Lipparini, F.; Egidi, F.; Goings, J.; Peng, B.; Petrone, A.; Henderson, T.; Ranasinghe, D.; Zakrzewski, V. G.; Gao, J.; Rega, N.; Zheng, G.; Liang, W.; Hada, M.; Ehara, M.; Toyota, K.; Fukuda, R.; Hasegawa, J.; Ishida, M.; Nakajima, T.; Honda, Y.; Kitao, O.; Nakai, H.; Vreven, T.; Throssell, K.; Montgomery, J. A., Jr; Peralta, J. E.; Ogliaro, F.; Bearpark, M. J.; Heyd, J. J.; Brothers, E. N.; Kudin, K. N.; Staroverov, V. N.; Keith, T. A.; Kobayashi, R.; Normand, J.; Raghavachari, K.; Rendell, A. P.; Burant, J. C.; Iyengar, S. S.; Tomasi, J.; Cossi, M.; Millam, J. M.; Klene, M.; Adamo, C.; Cammi, R.; Ochterski, J. W.; Martin, R. L.; Morokuma, K.; Farkas, O.; Foresman, J. B.; Fox, D. J. *Gaussian 16*, Revision A.03; Gaussian, Inc.: Wallingford, CT, 2016.

■ NOTE ADDED AFTER ASAP PUBLICATION

This paper was published ASAP on September 28, 2021, with an incomplete version of the Supporting Information file. The corrected version was posted October 12, 2021.